

Preparation in situ and characterization of zeolite enclosed nanoparticles

R. BOSÎNCEANU, F. IACOMI*, A. V. SANDU^a

Department of Physics, "Al. I. Cuza" University, 11, Carol I Blvd, 700536, Iasi, Romania

^aARHEOINVEST Platform, "Al. I. Cuza" University, 11, Carol I Blvd, 700536, Iasi, Romania

$\text{Fe}_3\text{O}_4/\gamma\text{-Fe}_2\text{O}_3$ modified single crystals zeolite LTA and natural clinoptilolite by treatment with urea/ FeCl_3 aqueous solutions under different experimental conditions were achieved. Our research involves a modified co-precipitation approach for the controlled growth of $\text{Fe}_3\text{O}_4/\gamma\text{-Fe}_2\text{O}_3$ nanocrystals within the superparamagnetic and single domains limits by creating the precipitating conditions with the help of the hydrolysis reaction of the urea. The resulting materials were investigated by powder- XRD, magnetic and the electrical resistance measurements. Room-temperature M-H measurements verify the influence of synthesis conditions and crystal size on the magnetic properties of ferrite nanocrystals. The structure of clinoptilolite (CLI) and Linde Type A (LTA) zeolites with channels and cages of dimensions at the molecular level was found to play the role of a template, controlling the size and distribution of the formed $\text{Fe}_3\text{O}_4/\gamma\text{-Fe}_2\text{O}_3$ nanoparticles.

(Received May 25, 2011; accepted September 15, 2011)

Keywords: ferromagnetism, Linde Type A (LTA), Clinoptilolite (CLI), Urea, Fe_xO_y , Nanoparticles

1. Introduction

Magnetic properties of nanoparticles are subject to intense research activity driven by a fundamental interest in the novel physical properties of the nanoscale system and also potential industrial application of nanostructured materials. This letter reports on the synthesis method of well-dispersed diluted magnetic semiconducting nanoparticles within an aluminous-siliceous matrix. The use of the zeolite LTA and CLI as self-assembled nanotemplates, enable us to synthesize composite materials containing magnetic oxides nanoparticles at different temperatures for magnetic properties optimization. Comparable inorganic methods for the synthesis of nanoscale mixed-metal oxides require heating at high temperatures in order to produce the desired oxide composition and microstructure [1, 2]. The development of such mixed-metal oxide and zeolite-based nanocomposites is targeting the functionalization into device technologies for sensors applications.

The materials challenge is to magnetize functional non-magnetic materials by synthesis dilute concentrations of magnetic species, thereby harnessing the benefits of a magnetic response without significantly affecting the desirable physical properties of the non-magnetic host.

2. Experimental Part

2.1. Starting materials

All the chemicals were reagent grade and used without further purification. The following materials were used for the preparation in situ of $\text{Fe}_3\text{O}_4/\gamma\text{-Fe}_2\text{O}_3$ on zeolites: synthetic zeolite LTA with pore size of 0.3-0.8 nm and natural clinoptilolite (CLI) with pore size of 0.4-0.7 nm

ferric chloride hexahydrate ($\text{FeCl}_3 \cdot 6\text{H}_2\text{O}$, >99%), ferrous chloride tetrahydrate ($\text{FeCl}_2 \cdot 4\text{H}_2\text{O}$, >99%), hydrochloric acid (HCl, 1N) were obtained from KEBO, distilled water and urea (46.66%).

In order to remove the impurities, the powdered natural clinoptilolite (Marsid, Romania) was submitted to an acid treatment, using a 1N HCl solution and thermally treated in their sodium cation form at 673K during 4h. The Fe/urea ratio was $R = 6; 10; 60$.

2.2. The construction of the ion exchange isotherms

The ion exchange isotherms for exchange of cations A and B in zeolites may be classified in five groups as given in Fig. 1 [6].

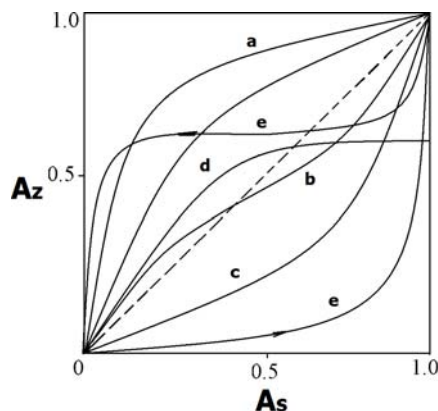


Fig. 1. Type of ion-exchange isotherm for the reaction $A_S + B_Z \rightleftharpoons A_Z + B_S$ (A, B are exchange cations in zeolite phase and solution, $A_Z + B_Z = 1, A_S + B_S = 1$) [6].

In curve "a", the zeolite exhibits a preference for the entering A ion ($\alpha_A^B = A_Z B_S / B_Z A_A > 1$ is the exchange degree) and the isotherm lies above the diagonal. In curve "c", $\alpha_A^B < 1$, and the isotherm lies below the diagonal indicating that B is much preferred. In curve "b", selectivity varies with the degree of exchange and resulted isotherm is sigmoidal in shape. Curve "d" indicate that the exchange is incomplete by the entering ion, due to the ion-sieving effect. Thus, $x_{\max} < 1$. In curve "e", unusual case is observed, where exchange results are in two zeolite phases and produce a hysteresis loop, [4].

In this paper the pretreating procedure for the natural clinoptilolite was performed according with Borros procedure [3]. A total exchange capacity of 2.87 meq/g CLI and of 5.5 meq/g LTA were taken in consideration in order to calculate the equivalent molar fraction. Fig. 2 and Fig. 3 presents the ion-exchange isotherms experimentally obtained.

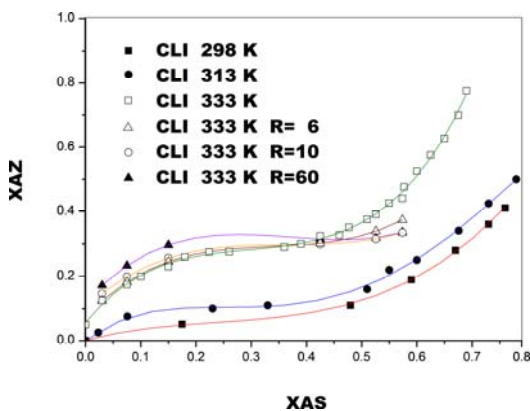


Fig. 2. Schematic representation of ion-exchange $Fe^{3+}-Na^{1+}$ isotherms for pretreated natural CLI ($T=298K, 313K, 333K$) and for treated natural CLI with urea ($R=6, 10, 60$). XAZ and XAS are the molar equivalent fractions of A cation in zeolite and solution phases.

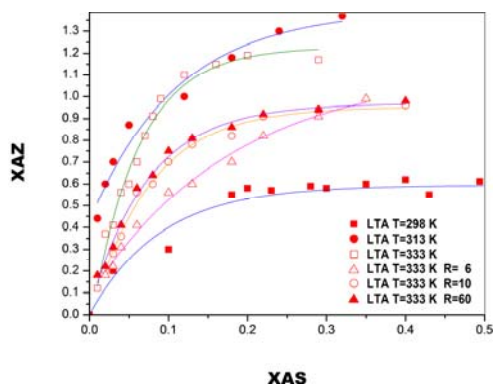


Fig. 3. Schematic representation of ion-exchange isotherms for zeolite LTA to ($T=298K, 313K, 333K$) and in the treated one with urea ($R=6, 10, 60$).

The type "b" isotherms indicate that the natural clinoptilolite prefers the Fe^{3+} ion only when is in contact with diluted solutions, as demonstrated by its downwards concavity. Since the inflexion point at 298K is almost

imperceptible, one might mistake this isotherm for one of type "c". Probably the Fe^{3+} has difficulty entering because of its quite large hydrated radius, close to micropore channel size. Observing the inflexion point, it can be concluded that these ions, even with a high charge, take on steric problems.

One of observation from Fig. 3 is that the isothermal behaviour is very similar with the type "d" for 298K and the type "a" for the rest. It is strongly hydrated at 298K, steric problems inhibit in some extent the retention of ferric ions. Possibly, at this temperature, Fe^{3+} cations are only located in the large cages due to the low XAZ values obtained for them.

It is also observed at 313K and 333K some over-exchanged values (the equivalent molar fraction of Fe^{3+} cation in zeolite phase $XAZ > 1$), which is probably due to some multilayer adsorption. A densely occupied monolayer will act in some degree as an extension of the zeolite, and will be able to attract further cations from the solution phase. XAZ values greater than 1 are possible to occur and the hypothesis of experimental errors should be completely discarded.

2.3 Construction of Kielland Plots

The Kielland quotients were obtained according to the equation:

$$\log K_c' = C_0 + 2C_1 X_{AZ}, \quad (1)$$

where

$$C_0 = \log K_B^A, \quad (2)$$

$2C_1$ is Kielland coefficient and K_c' is the corrected selectivity coefficient. X_{BZ} was considered to be:

$$X_{BZ} = 1 - X_{AZ}, \quad (3)$$

where BZ is the charge of the ferric ion, +3, and, supposing that only sodium ions are exchanged, ZA was considered to be +1.

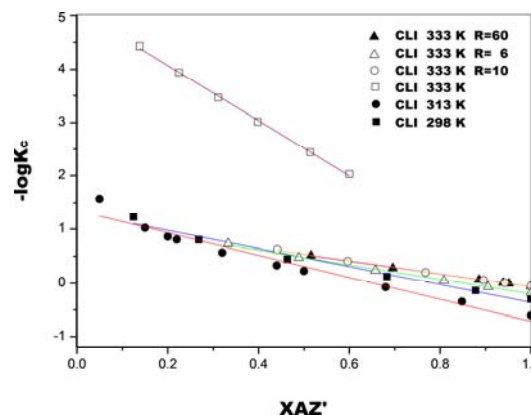


Fig. 4. Kielland plots for pretreated natural CLI ($T=298K, 313K, 333K$) and natural treated CLI with urea ($R=6, 10, 60$) for $Fe^{3+}-Na^{+}$.

The experimental points of the isotherms were fitted to equations and the functions $X_{AZ}=f(X_{AS})$ calculated with the help of the software package Table Curve and activity coefficients with PHRQPITZ program. In this way, the curve points were normalized and they were used to calculate K_c . Afterwards, Kielland plots were constructed and are presented in Fig. 4 and Fig. 5.

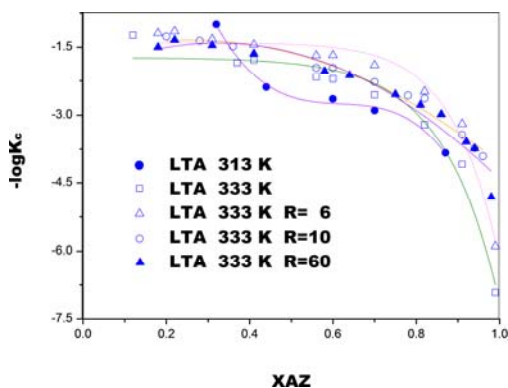


Fig. 5. Kielland plots for LTA zeolite to ($T=313K, 333K$) and treated LTA zeolite with urea ($R = 6, 10, 60$) for $Fe^{3+}-Na^{+}$.

With the ion exchange data it was possible to calculate the selectivity coefficients and the respective Kielland plot of each isotherm. The mathematical algorithm performed to obtain the Kielland plot improves the visualization of the straight lines. It indicates that the exchange sites have the same energy.

Nevertheless, the analysed mineral has three main kinds of exchangeable cations; hence, it should display several exchange sites of different energies. As the Kielland plots are linear, we believe that only one kind of site acts in the exchange process with Fe^{3+} cation. The straight lines present positive values of C_1 , indicating that the energy involved is an exothermic one and that the Fe^{3+} cations tend to cluster.

The degree of exchange increases as the temperature increases, because it apparently inhibits this tendency to cluster. It is observed that at the higher temperature, the distribution of the Fe^{3+} ions is more regular through the sites. Thus, the zeolite is able to shelter a greater quantity of these ions, modifying the inflexion point. All Kielland plots show non-linear shape for the Fe^{3+} cations investigated. This feature is typical for zeolite frameworks with distinct energies and LTA is in this category [5].

2.3. The determination of the optimum urea/ferric ratio

The pH change of each solutions at $R=6, 10$ and 60 with the reaction time are shown in Fig. 6. The pH rate rises rapidly with R and the final pH attains values comparable to base solution.

It was observed that the pH of solutions with $R = 6$ and $R = 10$ rises in a slowly way to a pH 4-5. This feature was not observed in the solution with $R=60$.

The products formation to distinct pH values from the solutions with $R=6$ and 60 is shown in Fig.7.

From the results of pH measurements, it was possible to establish the acid conditions, around pH 1-2, to produce β -FeOOH compound and around pH 4-6 to produce magnetite. α -FeOOH can be obtained only from the solutions with $R=6$. Magnetite and α -FeOOH were precipitated at the same time. One constate that α -FeOOH gradually decreased and transformed into magnetite. The $R=60$ condition do not allowe the formation of α -FeOOH. A small increase in R value determines a strong increase in the pH value and the magnetite precipitation process takes place suddenly.

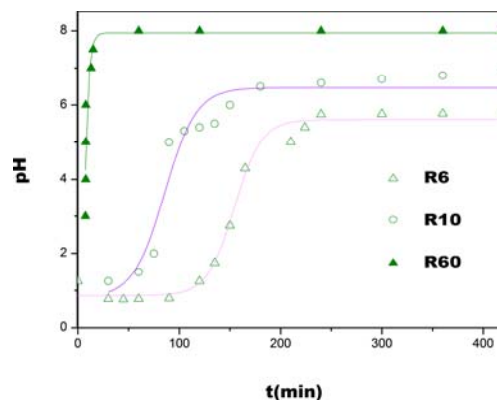


Fig. 6. The pH as function of reaction time for solutions at $R=6, 10, 60$ molar ratio

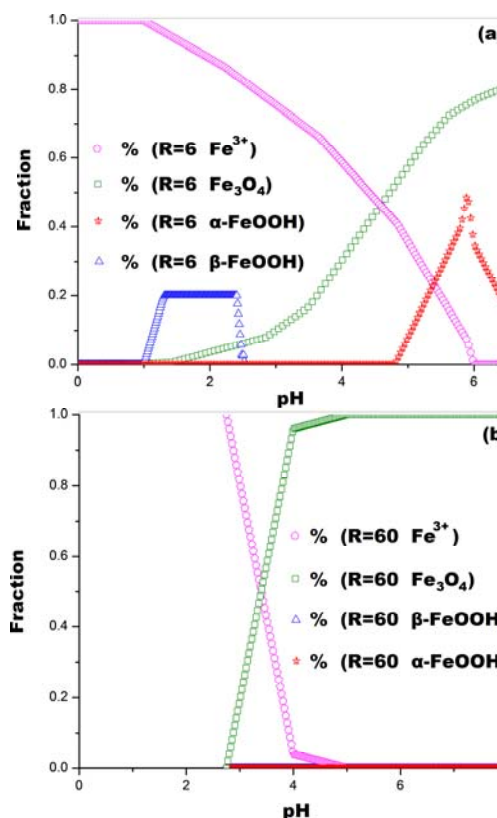


Fig. 7. The formation of Fe^{3+} , Fe_3O_4 , β -FeOOH and α -FeOOH to distinct pH values from solutions with (a) $R=6$ and (b) $R= 60$.

At small R values ($R=6$) the pH increase slowly and the urea hydrolysis imposes the formation of magnetite. During the magnetite precipitation process, the pH of the solution was kept at a constant value, about 4.6.

When R value was large, the rise rate of pH was fast and the pH value quickly reached about 7 - 8, being optimum ratio for the proposal goal.

2.4. The modified co-precipitation of $\text{Fe}_3\text{O}_4/\gamma\text{-Fe}_2\text{O}_3$ into zeolites

The chemical activation process of the zeolites realized on chemical and thermal way is: one gram of 200 mesh Na-LTA dried probe was annealed at 550-600°C in an air or nitrogen current for the removal of the network-forming organic molecules. The activated zeolites probes were washed with distilled water and dried at 105°C.

When the ionic-exchange isotherm indicates the pre-established concentration of the ferric ions, it adds ferrous chloride at 98°C, thereby it is realized the ferrous ions adsorption and according with Fig.7, the urea hydrolysis determine the rise of the pH to optimal values.

The co-precipitation direction is realized according the diagrams from Fig. 7 (a, b). For the urea excess hydrolysis and the anions removal, a 30 minutes treatment with steams at 120°C was performed.

The modified zeolite was 20 minutes dried with air at 105°C and annealed 20 minutes hour-long at 900 °C.

In these conditions were obtained zeolite samples with iron contents from 0.5 Fe^{3+} mEg/g zeolite until 2.2g Fe^{3+} /g zeolite. The codes of sample are: LTA0.5, CLI0.5, etc.

2.6. Characterization

The crystalline structure of the parent and modified zeolites was studied by the X-ray diffraction method. Powder XRD patterns were recorded by using a DRON 2 diffractometer ($\text{CuK}\alpha_1$ radiation, $\lambda=1.5405 \text{ \AA}$).

The crystal morphology of the parent and modified zeolites was analyzed with a scanning electron microscopy (SEM) VEGA II LSH TESCAN, connected with a EDX detector, QUANTAXQX2.

The Magnetic measurements were carried out by the vibrating sample magnetometer at the room temperature..

Measurements of the electrical resistance as a function of temperature were made in air, in the range of 293–473K by an experimental set-up using a KEITHLEY 6517A instrument. Pellets of 8 mm diameter and 2.7 mm thick were prepared by pressing of powder samples at 10 tf/cm².

3. Results and discussion

XRD diffraction patterns of the samples are shown in Fig.8 and Fig.9 and are typical for diffraction patterns of clinoptilolite and LTA zeolites.

There is no evidence of the FeO(OH) , (Fe_xO_y) , Fe_3O_4 , $\gamma\text{-Fe}_2\text{O}_3$, $\alpha\text{-Fe}_2\text{O}_3$ diffraction peaks in the XRD pattern of LTA samples with small contents of iron oxides. Some small shifts of XRD peak positions and changes in XRD

peak intensities are evident. These changes influence the unit cell parameter values of LTA (Fig.8).

Drastic changes are visible in the XRD pattern of sample LTA2.2 (2.2 mEg Fe^{3+} /1gLTA). High iron oxide contents determine a partial loss of host crystallinity and the formation of some iron (III) oxide nanoparticles, especially magnetite, Fe_3O_4 , lepidocrocite and FeO(OH) on the zeolite external surface (Fig. 7). These results suggest that the process of clusters formation involves the aggregation within the large cages of the parent zeolite LTA and the local destruction of the network pores.

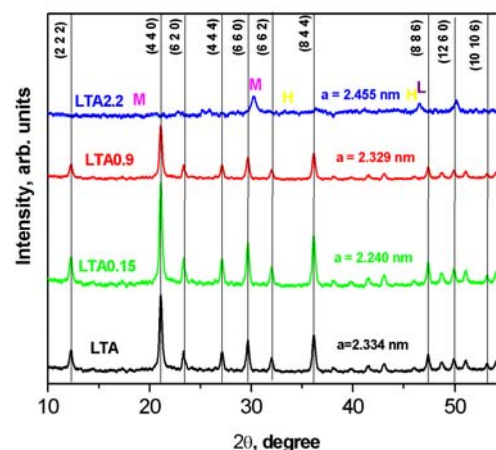


Fig. 8. XRD patterns of LTA samples with different contents of iron oxides.

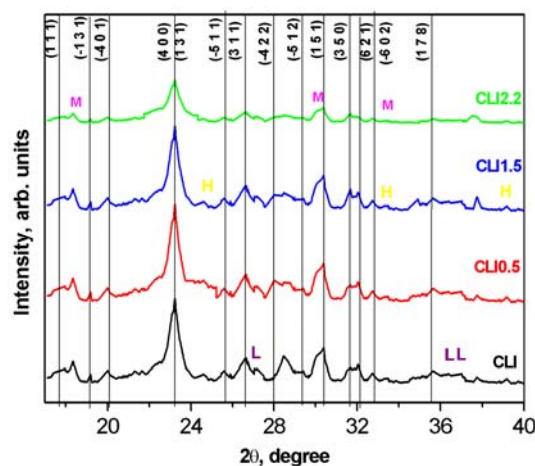


Fig. 9. XRD patterns of Na-CLI samples with different contents of iron oxides.

XRD pattern of clinoptilolite samples show the clinoptilolite characteristic peaks and also peaks belonging to different oxides and hydroxides (Fig.9). As in the case of LTA zeolite, iron oxides cause damages to zeolite framework during the annealing process.

The calculated unit cell parameters of CLI samples are presented in Tab.1. A dependence of their values on the chemical unit cell composition was evidenced

SEM images of microcrystalline Na-CLI zeolite and crystalline LTA and of iron oxide modified ones, confirm the fact that the zeolite frameworks crystallinity was maintained (Fig. 10. (a - d)).

There are several papers on describing the magnetic behavior of some natural and synthetic zeolites [7]. We report here the first results of the ferromagnetism at the room temperature for the dilute (<4 at.%) Fe_xO_y embedded zeolite LTA sample. The iron is found to carry an average magnetic moment of 0.16 $\mu B/ion$

Tab. 1. XRD structural characterization of Fe_xO_y - CLI

Sample s	Fe^{3+} mEg/1g	a(Å)	b(Å)	c(Å)	β	V(Å ³)
CLI	-	17.82	18.64	7.3	115.1	2100.8
CLI0.5	0.5	17.81	18.65	7.29	115.1	2101.7
CLI1.5	1.5	17.76	18.67	7.28	115.9	2229.4
CLI2.2	2.2	17.66	18.76	7.27	115.7	2198.7

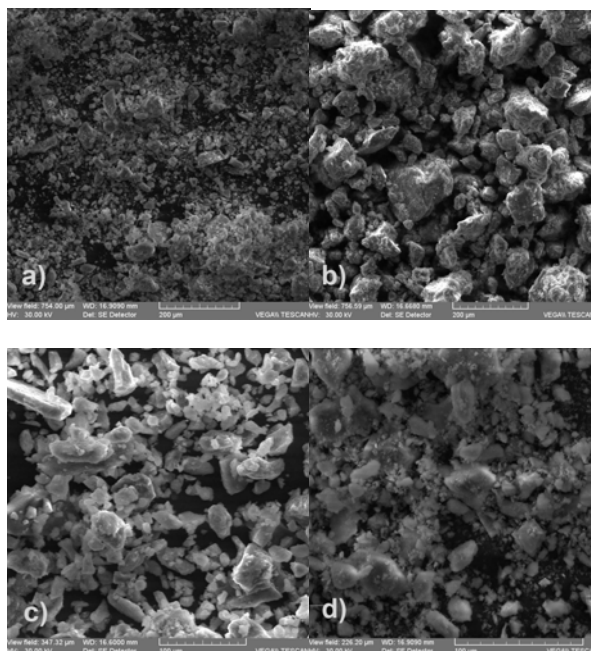


Fig. 10. The SEM micrographs of a) the parental LTA zeolite, b) the LTA1.5 zeolite, c) the parental CLI zeolite, d) the CLI1.5 zeolite.

It was found that iron atoms are predominantly in the Fe^{3+} ionic state into the channels and cavities of zeolites. Small amounts of iron oxides were evidenced only for samples containing 2.2 mEg $Fe^{3+}/1g$.

The VSM measurements at room temperature, indicate that LTA2.2 sample exhibits ferromagnetic behavior with characteristic parameters as saturation magnetization, M_s , of 8 emu/g and coercivity, H_c of 100 Oe.

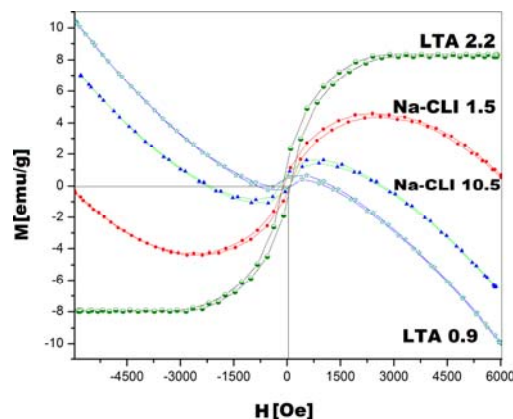


Fig. 11. VSM magnetization curves of samples

The electrical conductivity of the zeolites in their cation forms and the diluted magnetic semiconductor nanoparticles encapsulated in LTA and CLI zeolite was studied as a function of temperature.

The formation of semiconductor clusters into the zeolite channels (CLI) and cages (LTA) determines the increase in electrical conductivity and a sharp decrease in the activation energy (Fig.12, Tab.2). The differences in E_a values, calculated from the dependence $\sigma=f(10^3/T)$, can be related with the substitutional or interstitial Na impurities.

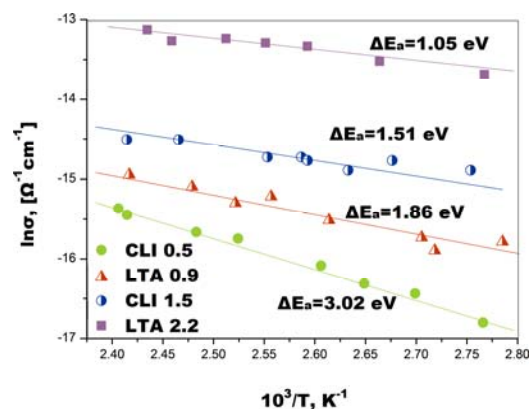


Fig.12. The electrical conductivity as a function of temperature

The changes in electrical properties are due to transformations in the density of electronic levels as a function of the size, known as quantum size effects.

5. Conclusions

The synthesis of some iron oxide nanoparticles into the channels and cavities of clinoptilolite and LTA zeolites was optimised by controlling the solution pH and R values based on ion-exchange isotherm analysis.

In situ prepared iron oxide nanoparticles exhibit interesting electrical and magnetic properties, comparable with other once isolated in other matrices.

Iron oxide nanoparticles exhibit a superparamagnetic

behaviour and display little remanence and coercivity while keeping a high saturation magnetization.

References

- [1] R. Bosînceanu, N. Sulişanu, J. Optoelectron. Adv. Mater. **10**, 482 (2008).
- [2] C. Weidenthaler, B. Zibrowius, J. Schimanke, M. Yachun, B. Mienert, E. Bill, W. Schidt, Microp. Mesop. Mater. **84**(1-3), 302 (2005).
- [3] M. A. S. D. Barros, A. S. Zola, P. A. Arroyo, C. R. G. Taveira, E. F. Sousa-Aguiar, Adsorption **12**, 239 (2006).
- [4] R. M. Barrer, J. Klinowski, Theory of Isomorphous Replacement in Aluminosilicates, Phil. Trans. R. Soc. Lond. (1977).
- [5] F. Iacomi, Surf. Sci., **532-535**, 816 (2003).
- [6] Breck, D. W. Zeolite Molecular Sieves: Structure, Chemistry and Use." Wiley, New York, pp. 771, (1974)
- [7] V. Pode, E. Popovici, R. Pode, V. Georgescu, Rev. Roum. Chim. **52**(10), 983 (2007).

*Corresponding author: f_iacomi@yahoo.com